VOL. 18, NO. 4, FEBRUARY 2023 ISSN 1819-6608
ARPN Journal of Engineering and Applied Sciences

www.arpnjournals.com

TOWARDS A DETAILED URBAN STRUCTURAL MAPPING USING OUTCROP, GEOPHYSICAL AND BOREHOLE DATA INTEGRATION: IMPLICATIONS FOR SUSTAINABLE DEVELOPMENT

Ahmed Henaish[1], Mohamed Attwa[1,2], Mohamed Elnahal[1] and Kareem Mohsen[1]
[1]Department of Geology, Faculty of Science, Zagazig University, Zagazig, Egypt
[2]National Authority of Remote Sensing and Space Sciences, Cairo, Egypt
E-Mail: attwa_m2@yahoo.com

ABSTRACT

Nowadays, geological conditions and geohazards assessment are essential requirements for sustainable urban planning and development. Hence, with lack of outcrop and near-surface geology, additional geohazards can be imposed. The present study is the first such challenge in one of highly deformed areas in Egypt and, accordingly, an integrated approach for detailed urban geological and structural mapping is given. Therefore, the surface and subsurface field measurements converge on the detailed geological conditions characterization including structural settings in a new urban city, as a case study. In this regard, the measured surface structural data are presented on a detailed geological map considering the surface rock units geometry and distributions. In order to unravel the near-surface geology, geophysical direct current resistivity (DCR) sounding survey is performed to represent subsurface layers distribution considering the surface geological mapping. To reduce the limitations of DCR sounding interpretation, conventional and non-conventional inversion schemes are applied with reference to available borehole data. Evidently, the sum of surface and near-surface mapped fault segments are plotted and analyzed to provide a detailed geometrical structural model. Because the fault rupture hazards and shale layer expansion issues are closely related to the urban sustainable development, a preliminary geohazards assessment is illustrated in the form of fault setbacks calculation and the shale free swelling evaluation. The present approach provides a holistic view of the urban geological mapping and introduces a means of recognizing preliminary potential geohazards problems and/or opportunities at an early stage in any proposed sustainable development, which can support site investigation designing strategies.

Keywords: urban geological mapping, DCR soundings, genetic algorithms, structural mapping, fault setback, Cairo-Suez district.

1. INTRODUCTION

Because the population is rapidly increasing, the urban areas are growing throughout the world. Obviously, desert lands are being transformed due to the rising demand for urban expansion to sustain residential and commercial activities (1). Regarding to the United Nations report launched in 2019, world population in 2050 is expected to reach 9.7 billion. Moreover, the sub-Saharan Africa population is projected to double by 2050. On the other hand, regions that possibly will experience lower population growth rates between 2019 and 2050 include Oceania excluding Australia/New Zealand, Northern Africa and Western Asia, Australia/New Zealand, Central and Southern Asia, Latin America and the Caribbean, Eastern and Southeastern Asia and Europe and Northern America (2). Accordingly, the study of geological hazards and land resources, i.e., urban geology, are necessary for the expansion and development of new urban areas (3). More recently, environmental geology and/or urban geology have attracted attention to avoid the urban environment degradation and geo-environmental hazards which threaten the new urban cities (4), (5). In briefly, key considerations for sustainable development in new urban areas are economical design, stability and safety.

Geohazards are related to the geological/structural settings and soil conditions which capable of causing damage or loss life (6). Furthermore, insufficient data about the subsurface geological structures complicates the subsurface composition which in turn provides significant geohazards. Consequently, the data bases establishment covering all existing surface and subsurface information is a critical requirement for the urban land use planner's support. In consequence, the geological and structural assessments of rational urban planning and development can considerably improve society resilience to geohazards.

Within the urban geology framework, structural and geotechnical mapping can provide geotechnical parameters to establish a suitable map for safe urban expansion and rational development planning (7). In addition, surface geological and structural mapping are based, conventionally, on literature data, geologic field reconnaissance and field stratigraphic and structural information (8), (9). Similar works on urban geology and geo-risk assessment have been undertaken using remote sensing (RS), GIS and multi-criteria decision analysis (10), (11). However, the field geological formations recognition as well as their tectonic character always remains a risky mission for any precise geological mapping. Accordingly, the integration of RS, GIS, surface geological and structural information and subsurface data are essential for detailed urban geological and hydrogeological mapping of highly deformed areas (12), (13).

Deeper in the subsurface, the heterogeneities and structures may cause urban environment instability. In

ARPN Journal of Engineering and Applied Sciences

general, the conventional drilling is high cost and time consuming particularly in regions where boreholes density is low. In contrast to traditional drilling, the subsurface geology and structures information applying in-situ geophysical techniques is non-destructive giving faster results (14), (15). Over the years, the failure of many urban development projects and the desire to reduce the borehole drilling has led to application of geophysical techniques as a prerequisite to any successful urbanization project and integrated geophysical approaches even play a more decisive role in urban geology investigations. Direct ground-based geophysical methods are able to acquire the physical parameters linked directly or indirectly with the lithological and geotechnical characteristics (16). Among the geophysical methods, geoelectrical methods have been increasingly applied to geological, structural, landslide and hydrogeological mapping (17), (18), (19). In recent times, direct current resistivity (DCR) sounding survey has been effectively applied to geological, geotechnical and hydrogeological assessment (20). (21) pointed out that DCR soundings are not destructive and can effectively provide valid field geological data in arid areas for geological and structural mapping in a cost-effective way (22).

Keeping these in view, the purpose of the present case study is to introduce an integrated approach for urban geological mapping in desert lands using detailed geological, structural and geophysical data. In this paper, we adopted DCR sounding survey to obtain meaningful subsurface geological information to support and supplement other surface geological and structural data. The use of field geophysical data with the geological and structural studies make it possible to recognize the spatial geological characteristics and provide a better understanding of geologic hazards from the viewpoint of structural geology.

2. GEOLOGICAL AND STRUCTURAL SETTINGS OF THE STUDY AREA

The Cairo-Suez District (CSD) is considered as one of the most attractive places for land reclamation projects and quick expansion in urbanization (Figure-1a). Additionally, numerous new communities have been established (e.g., El Obour, New Cairo, Badr, 10th of Ramadan and El Shorouk). However, awareness should be considered in such desert areas because of its complicated geological and structural setting (23), (22), (24), (25), (26).

From tectonic standpoint, the CSD represents a partition of the unstable shelf area which extends at most of northern Egypt. Several tectonic events have been encountered along CSD associated with the movements between the Eurasian, African and Arabian plates (27). These tectonic episodes include a rifting phase during the Jurassic-Early Cretaceous periods that was responsible for forming the Tethyan passive continental margin (28). Consequently, the E-W trending deep seated faults have been reactivated along the CSD. During the Late Cretaceous period, the majority of E-W oriented faults were reactivated by dextral movements (29). Another phase of extension came upon the Late Oligocene to Early Miocene times which associated with the Gulf of Suez rift and continued to the post-Miocene period. Because the Gulf of Suez rift was incapable to extend north of the Suez City (Figure-1a), the throw on the faults was transferred into the CSD (30) throughout the deep seated E-W faults. As a result, rejuvenation by dextral transtension led to forming E-W elongated belts of left-stepped en echelon normal faults (31) as well as NW-SE oriented normal faults.

From structural geology perspective, two provinces can be related to the CSD in relation to Cairo-Suez road (CSR), Figure-1a. Such provinces are portrayed by several uplifted blocks and down faulted sub-basins. In fact, faulting movements played the major role in determining the distribution and lateral facies changes between the different outcropped rock units along CSD which range in age from Cretaceous to Recent. The northern province (i.e., north of CSR) is characterized by folding and faulting affecting Cretaceous, Eocene, Oligocene and Miocene outcrops (e.g., G. Shabraweet; G. Umm Raqm; G. Hamza; G. Um Qamar), (Figure-1a). Contrarily, the southern province (i.e., south of CSR) is portrayed by several notable Eocene fault blocks (e.g., G. Ataqa; Qattamiya; G. Abu Shama), (Figure-1a). The CSD is an eminent locality of fault belts (FB) which encloses diverse fault geometries (32), (7), (33) (Figure-1a). In addition, such fault belts comprise zones of low to moderate seismicity (34) (e.g., Abou Elenean *et al.,* 2010). Hence, from engineering viewpoint, such fault belts open major engineering and environmental hazards. Formerly, (31) documented four en echelon fault belts that involve the CSD (Figure-1a), which are; (i) Shabraweet-Um Qamar FB, (ii) Oweibed FB, (iii) Ataqa-Qattamiya-Maadi FB and (iv) North Galala fault FB.

The study area (New Obour City) represents a new community, which is the eastern continuation of El Obour City (Figure-1a). General speaking, El Obour City can be considered as one of the largest newly urbanized communities in the region of CSD. Obviously, the accommodation challenge in El Obour City is becoming more difficult in adequate housing especially with urban sprawl. Accordingly, New Obour City (Figure-1b) is established as a promising city with ambitious development plans. As a desert land, the study site is characterized by significant variations in geological settings, topography and structures. From a geological viewpoint, the shale layers are situated near the surface (Figure-1c) with various thicknesses and, accordingly, engineering and environmental precautions have to be considered especially with urban expansion. Moreover, the investigated area occupies the western extension of Shabraweet-Um Qamar FB. In this manner, geohazard impact of such complicated structural zone on urbanization should be taken seriously. Accordingly, a detailed urban geological mapping, considering both surface and subsurface geology, has a considerable engineering and environmental impacts.

Geologically, New Obour City involves a part of the Obour-Orabi sub-basin and belongs to the Gebel Um Qamar region (Figure-1a). The surface geology of the

ARPN Journal of Engineering and Applied Sciences

study area is represented by three main lithostratigraphic units (Figure-2) namely; Marine Miocene Unit, Non-marine Miocene unit and Quaternary sediments. The marine Miocene rocks (36) comprise sandstone intercalated with shale beds, argillaceous sandstone and sandy limestone beds. This is followed by the sands and gravels which are shaly in parts of the non-marine Miocene unit (36). Quaternary sediments cover a large portion of the area comprising sands and gravels are well exposed at the southern part of the area that overly the non-marine Miocene rock unit. Regarding to the aforementioned geology, the near-surface heterogeneities and shale layer distributions are highly required for detailed urban geological mapping and safe urban expansion in the study site.

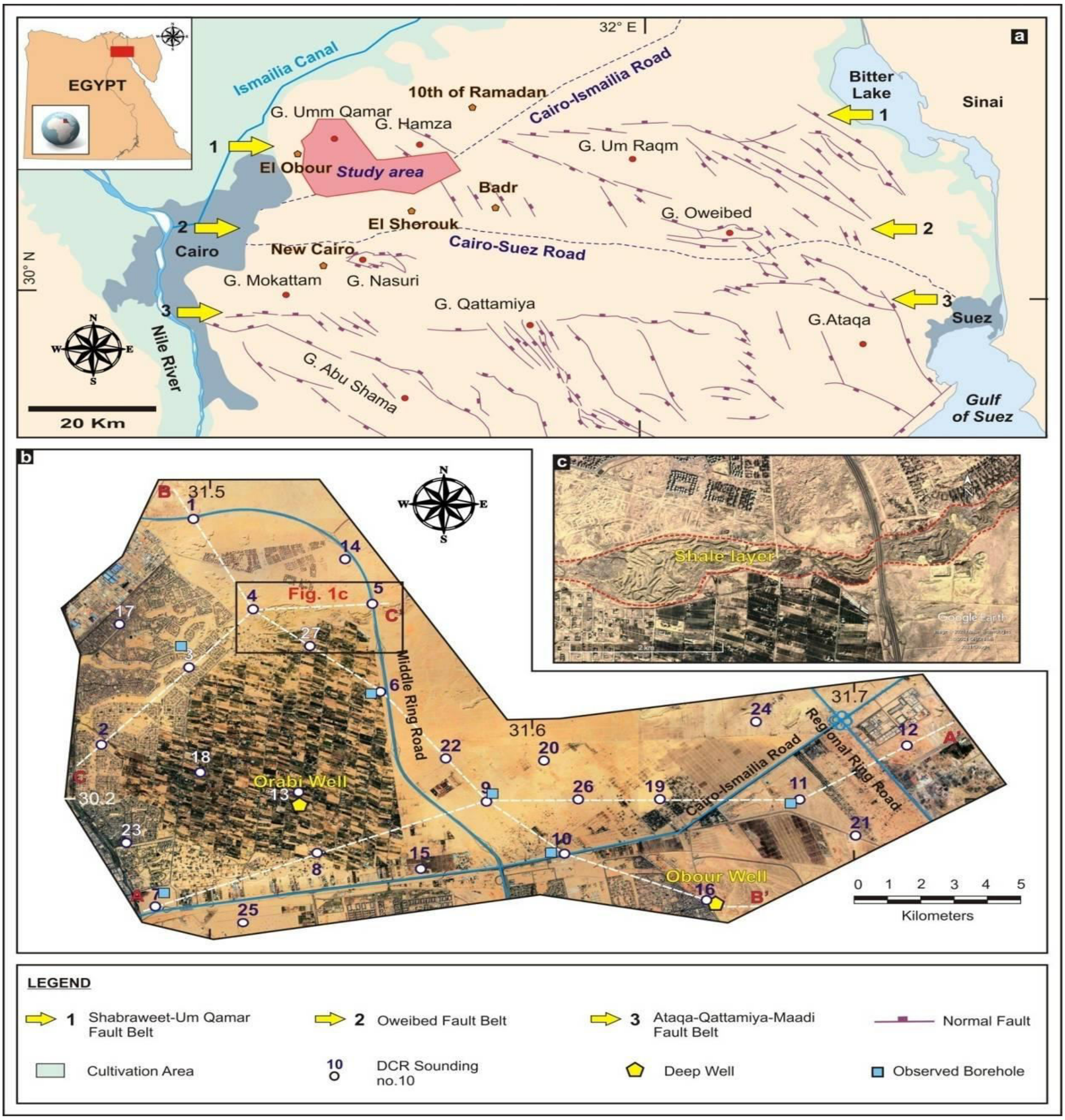

Figure-1. (a) Simplified tectonic map of Cairo-Suez District (CSD), the compiled major structures (37), (38), (22). (b) Google Earth image shows the study site and DC resistivity soundings and boreholes locations. (c) A Google Earth image shows a surface shale layer at the northern part of the area. Note, the white dashed lines represent the location of the constructed stitched resistivity sections (A-A', B-B' and C-C') passing through the measured DCR soundings.

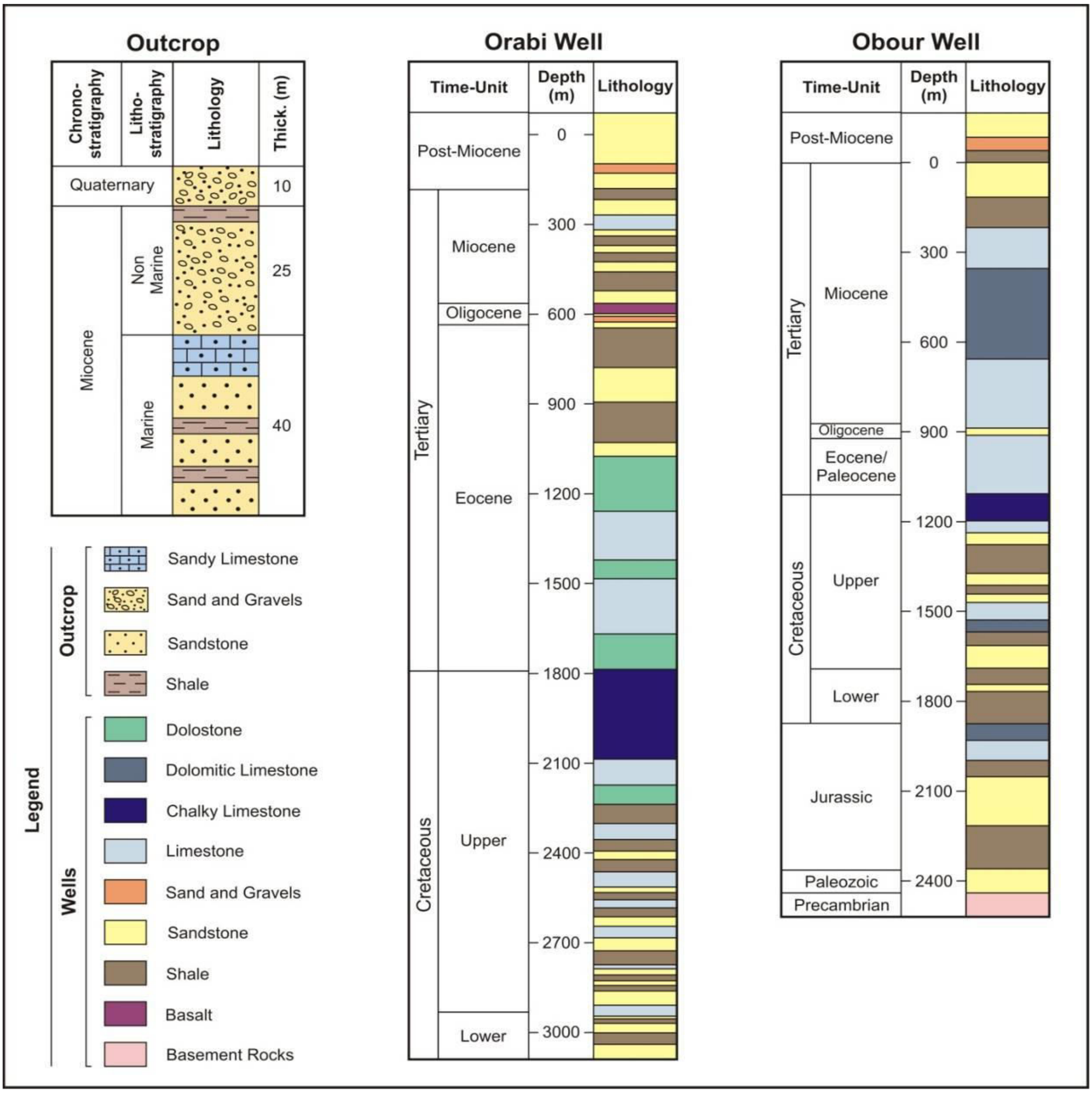

Figure-2. Stratigraphic setting of the study area in the form of outcrop measured composite section and drilled deep wells (35).

In the present study, surface structural mapping was started through a preliminary investigation of high resolution satellite images in order to delineate regional structures. This was followed by a detailed field-work via tracing geological structures. During this phase, location and geometric elements of the geological structures have been measured and recorded (Figure-3). Additionally, the interpreted structures based on investigated satellite images, were confirmed in the field. Where possible, displacement along the investigated faults has been measured. Finally, faults have been classified according to their types and attitudes and were plotted on their accurate locations on the prepared geologic map (Figure-4).

Based on the abovementioned structural data acquisition, the constructed geological map revealed that the measured dip values of bedding planes show a gentle dip that ranges from 6-12° towards the NW direction except for minor localities where bedding planes are tilting toward the SE (Figure-4). In addition, normal faults are the main structures that dissect the rock units at the whole area (Figures 3 and 4). The measured dip data from eleven fault surfaces indicated a moderate to steep angle, which generally exceeds 60°. The collected structural data during fieldwork revealed a sum of twenty-two mapped surface faults which belong to two ordinate sets oriented in a descending order of frequency; WNW-ESE and NE-SW with a subordinate orientation towards the ENE-WSW direction (Figure-4).

The subsurface geology of the Orabi basin is represented by two drilled deep wells namely; Orabi and

ISSN 1819-6608
ARPN Journal of Engineering and Applied Sciences

Obour wells (Figure-2). The Orabi well is located at the western part of the area and measures about 3238 m depth. It includes rock units that range in ages from Lower Cretaceous, to post-Miocene. Moreover, the Obour well is located at the southeastern part of the area where it represents a section of about 2700 m thick. This section starts with Precambrian basement rocks at the bottom and ends up with post-Miocene sediments. (35) indicated that the rock units of the Obour-Orabi sub-basin were deposited within a highly tectonically active zone. The inspection of such deep wells (i.e., Orabi and Obour wells) reflects considerable variations in geologic unit lithology and thicknesses (Figure-2), which can be conjugated with the local structural setting of the area. Moreover, it can be noticed that the Non-Miocene sediments are dominated at the northeastern part of the study site. On the other hand, the thickness of Marine Miocene sediments increases at the southeastern parts of the investigated site. Accordingly, mapping the subsurface structures is necessary to avoid geohazards considering the spatial variations in seismicity characteristics of the study site. Hence, preliminary construction site safety rules can be achieved.

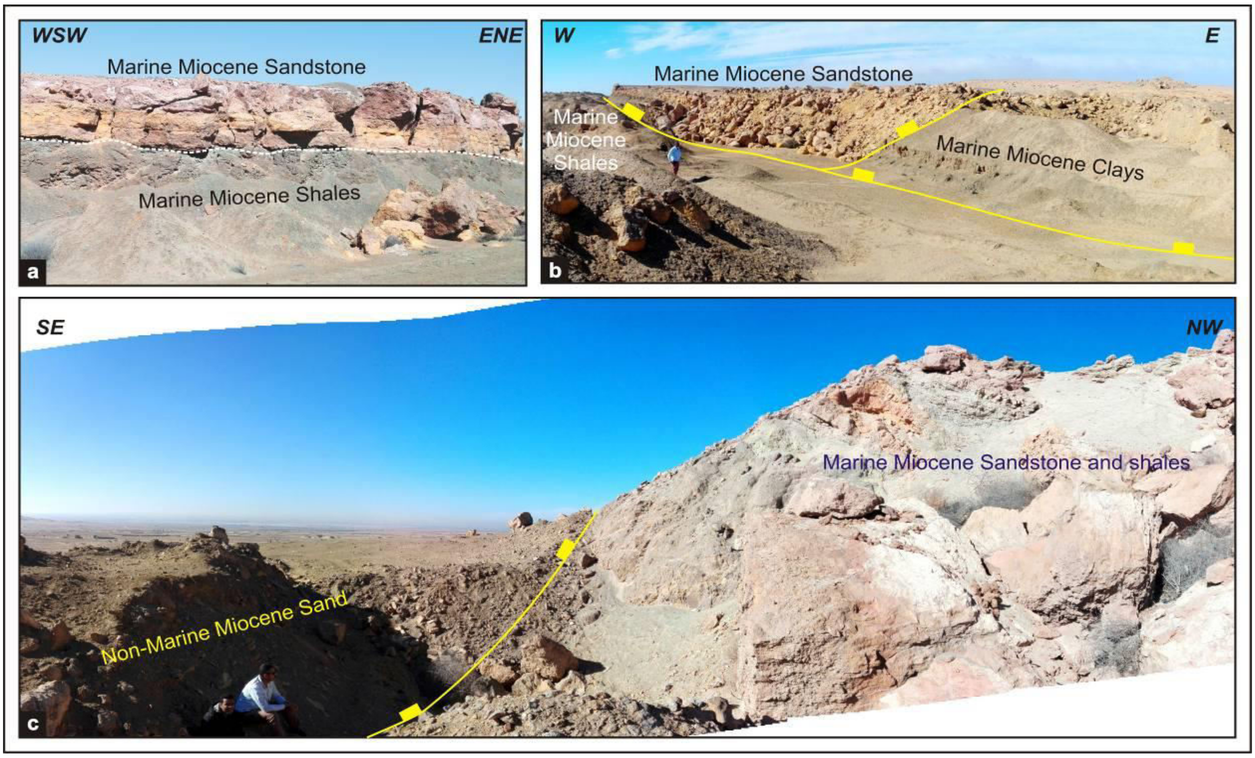

Figure-3. Outcrop examples of the exposed rock units and the recorded geological structures. (a) NW-dipping strata of the marine Miocene layers. (b, c) Normal faults affecting marine and non-marine Miocene sediments.

VOL. 18, NO. 4, FEBRUARY 2023 ISSN 1819-6608
ARPN Journal of Engineering and Applied Sciences

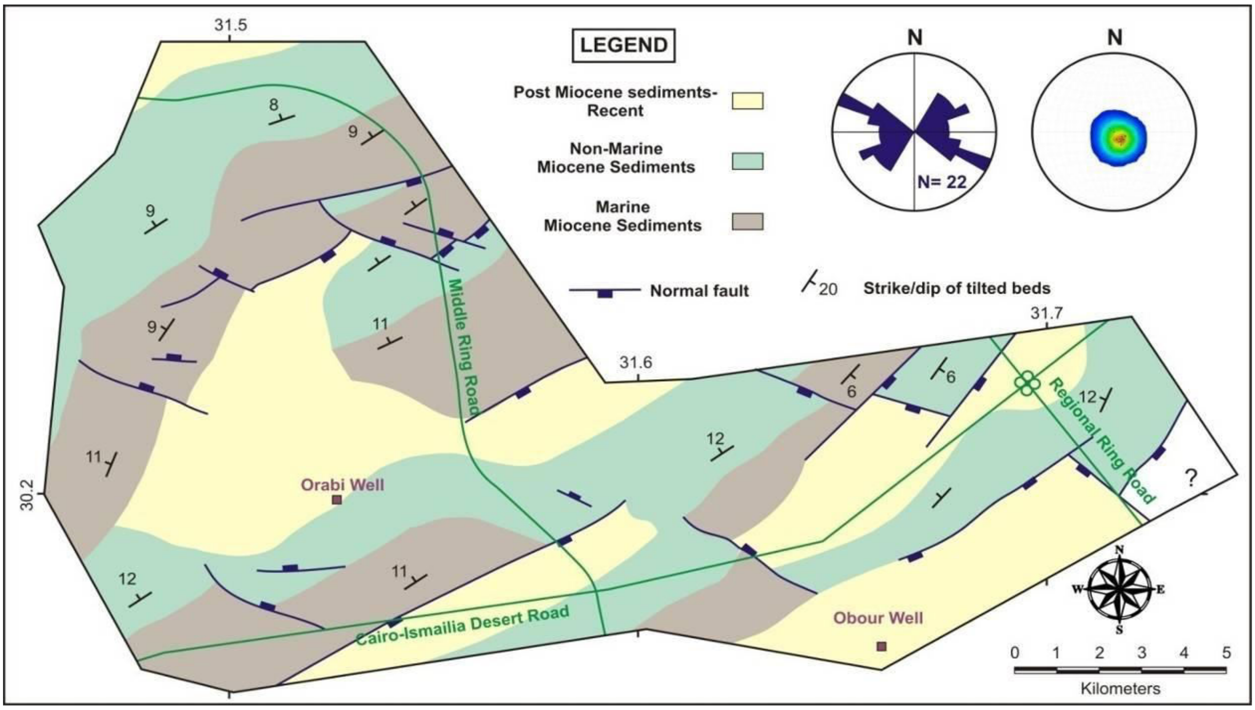

Figure-4. Surface geological map of the study area with a stereonet representation for poles to bedding planes and a rose diagram for Surface mapped fault attitudes.

3. METHODOLOGY

Obviously, understanding the geological and structural conditions of a new urban area is a substantial task especially at the desert lands, before its urbanization. Regarding the previously presented geological and structural studies, the tectonic structures and geological hazards related to surface faults and shale layers existence can be tracked and mapped. Accordingly, the geotechnical problems can be avoided at areas more vulnerable to geohazrds. Moreover, it can be noticed that Figure-4 can address preliminary engineering ground conditions and other geologic-related issues of the superficial deposits in a representative way to discuss the utility and limitations of the sustainable development (e.g., foundations conditions; excavatability) in the reclamation of a new urban area. Nevertheless, it is worth mentioning that the surface geological and structural information has to be complemented by subsurface data in order to build-up a detailed geometrical structural model representing the bedding planes geometry. Next, borehole and geophysical data are acquired considering the aforementioned surface geological and structural studies to represent a detailed geological map that can be used for a preliminary urban planning amidst reclaiming desert lands.

3.1 Geophysical Survey

As a depth-sounding technique, the geophysical data were acquired by applying 1D-DCR technique, which is widely used to construct sensible geological and structural models in a cost effective way (39), (40). For urban geological mapping, the eventual aim of geophysical measurements is to characterize the subsurface layers resistivity distribution depending on the surface apparent resistivity measurements. Then, the measured resistivity data are interpreted in terms of subsurface geology and structures calibrated with available borehole, geological and structural data (41), (42).

In general, the DCR technique requires electrical currents injection into the subsurface layers by a pair of current electrodes (AB). Then, the resulting variations in electrical potential are measured at other pairs of electrodes (MN). Accordingly, the subsurface resistivity variations can be measured. In a DCR sounding survey, the apparent resistivity values of subsurface layers with depth depending on the distance between AB spacing can be measured in one dimension. Twenty-seven DCR soundings were acquired (Figure-1) using conventional Schlumberger array with maximum AB spacing of 2000 m. (40), (43) indicate that it is better to use Schlumberger array in desert environment to obtain valuable information with good signal-to-noise ratio and resolution about the subsurface. In view of aforementioned geological and structural aspects, this electrode spacing is sufficient to reach the required depth that fulfills the urban geological mapping. The DCR soundings were measured, as possible, over a straight survey lines to reduce the DCR ambiguity relating to the ground surface topography. The precise locations and elevations of DCR soundings were acquired using a 2 m accuracy GPS unit. Moreover, some of DCR soundings were measured near to the observed boreholes for verifying/robust the DCR interpretation. As a desert land, the DCR sounding survey was carried out based on the land accessibility avoiding many hills and quarries. Accordingly, the DCR soundings distributions were irregular and/or the grid-like shape was not applicable (Figure-1b).

The DCR soundings were acquired using SYSCAL Pro resistivity meter (IRIS instrument). As a new urban area entry to reclaim, the ground surface is characterized by arid conditions and a relatively high resistance contact. Consequently, stainless steel electrodes were used with saltwater and bentonite, in a hole, around poor electrodes contact. The ground contact resistance (RS check) was less than 5 kΩ. The measured (i.e., apparent) resistivity data were stacked 8 times and final data were recorded when the data quality factor values were minimized (i.e. stacked error ~< 2%). Further, the measurements of standard deviation below 4% were used for interpretation process. The measured DCR resistivity values were edited by removing the faulty measurements. The field resistivity data with insignificant current and/or high standard deviation (> 4%) were excluded. Additionally, outliers of apparent resistivity values were rejected as bad data quality.

Inversion of DCR soundings has been carried out to get multiple true resistivities and thicknesses layer model. Regarding the geological information of the nearby boreholes, the true resistivities are well related to the local lithology of the study site. To reduce the uncertainty of DCR interpretation, conventional and non-conventional DCR inversion techniques were applied for robust DCR soundings inversion process considering the borehole information and geological/structural settings. For conventional inversion scheme, the DCR soundings were inverted as an initial step applying a sequential interpretation method depending on a 1D- linear filtering and damped least-squares algorithm (i.e., Levenberg-Marquardt). The sequential method is automated inversion algorithms proposed by (44). The measured DCR soundings were interpreted by the calculation of initial guess with improving the layer parameters in an iterative manner. The measured resistivity data were smoothed using the 1D smoothness weighting schemes.

The weight coefficients numerical values indicate the probability of a perfect fit (unity) and an infinite divergence (zero) between both data sets (44). Considering the conventional inversion results, non-conventional inversion process was carried out applying the genetic algorithms (GA) using a heuristic search and best low misfit value solutions selection (45), (46). GA is a flexible technique that can be applied and/or modified depending on the requirements imposed by the problem. Obviously, GA applications have become more common with increasing the computer's speed (47). Here, the biological evolution basic tools are applied such as reproduction, mutation, crossover and natural selection (48). In GA, the first generation consists of randomly generated parameter sets attributing to a chosen conceptual model. The parameters in the subsequent generations are modified by mutation and crossover operations. Based on Darwin's theory, the models producing lowest misfit values will have more survival chance in the next generation. As a final point, the GA locates a number of solutions in the global minimum neighborhood. If global minimum is in the predefined search space, the global minimum can then be traced. Accordingly, the parameter search space is progressively shrunk through successive generations. Finally, an accurate and/or specific solution can be selected based on other information (e.g., borhole data, geology) and/or in order to in accordance with the personal judgment of the interpreter, who takes into account the nature of the experiment. Accordingly, the final results of each DCR sounding curve represent geoelectrical layers with their attributing to resistivities and thicknesses.

An example of the interpretation of DCR sounding No. (9) is given in Figure-5 (for location, c.f. Figure-1). The layers number was derived from the borehole and local geological information. Note that the generation numbers and population size were both 50 (Figure-5a). Moreover, the mean and best misfits variation versus generation was illustrated (Figure-5a). Figure 5a indicates that the smallest and average values decrease very rapidly, which can be attributed to noise contamination of field data. Obviously, the smallest misfit at each generation cannot be reduced below a certain value (i.e. generation is more than 45). At the best misfit, a good fit between the measured and calculated data can be observed (Figure-5b). In detail, (45) explained the model response function and error energy map. Moreover, a good calibration between the borehole information and DCR inversion results applying GA can be noticed (Fig. 5c). Accordingly, it is preferable to incorporate the well-known borehole information to delineate the subsurface layer distributions and, as a result, the subsurface structures can be represented from the constructed geoelectrical cross-sections.

3.2 Data Integration

Outcrop collected and analyzed data are useful where integrated with DCR and borehole data to control the interpretation which in turn can provide more accurate urban geological mapping. Here, all the previously measured structural parameters are used after constructing the overall integrated structural model in order to throw the light on the precautions that should be considered when set up constructions and/or infrastructures near the mapped faults. Such precautions are related to uncontrolled surface fault rupture hazards. Hence, fault minimum setbacks are calculated for both hanging-walls and footwalls of the mapped faults.

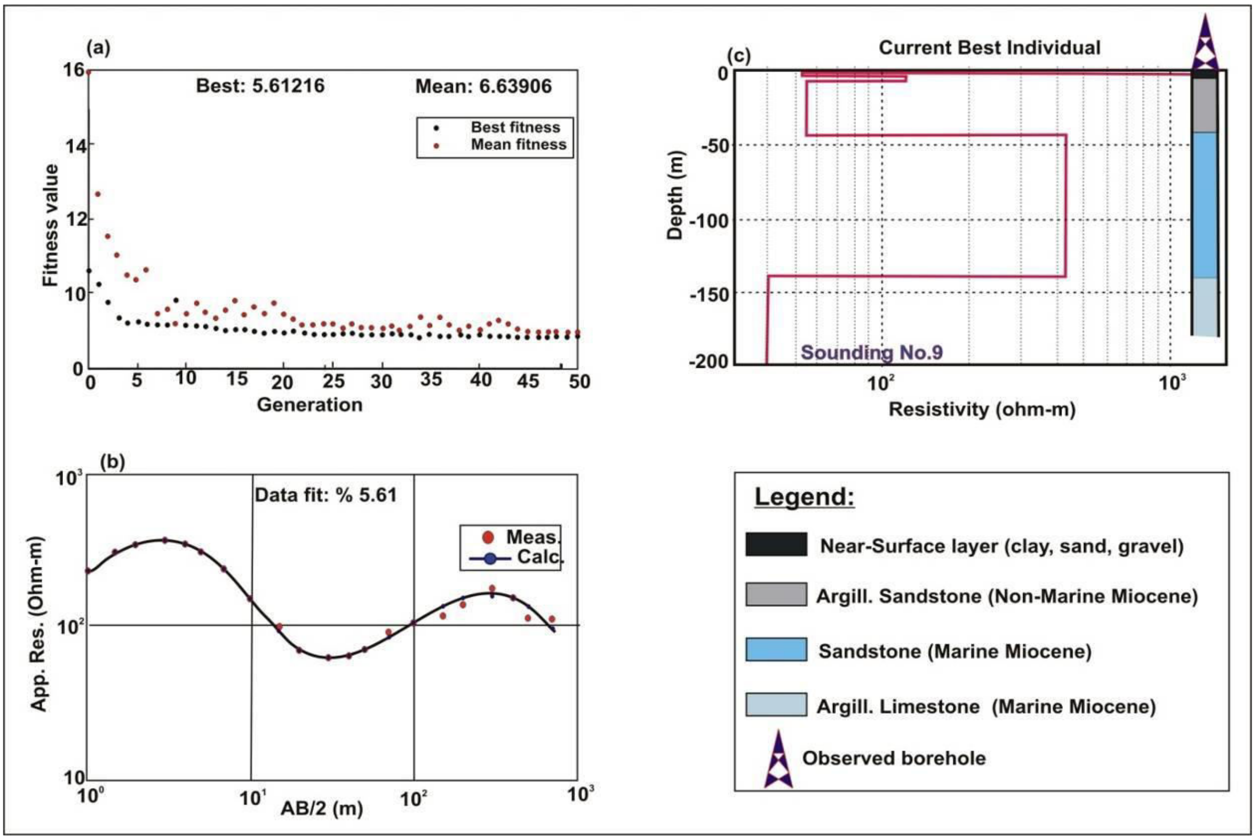

Figure-5. Interpretation of DCR sounding No. 9 (for location, c.f. Figure-1) with borehole data calibration using GA. The population size and generation number were 50. (a) Variation of mean and best misfit versus generation; (b) A comparison between the measured and theoretical data at the best misfit value; (c) A comparison between the model response resulting from GA and the borehole information.

4. RESULTS AND DISCUSSIONS

4.1 Detailed Urban Geological Mapping: A Geological/Structural Model

As aforementioned, the DCR inversion results were validated by surface geological/structural mapping and borehole data. In order to represent subsurface layer distributions, lateral geometric characteristics and a conceptual subsurface structural model, three stitched resistivity sections were established (A-A', b-b' and c-c', Figure-6). It is worth mentioning that the surface topography and the abovementioned geological and structural data (e.g., dip and strike, Figure-3) were considered in constructing the geoelectrical cross-sections (vertical exaggeration was adjusted by making Z= 4X and 8X). Moreover, to afford consistent stitched ressivity sections, the integrated approach after (22), (7) were applied where the geometrical parameters of bedding planes. Moreover, the observed fault planes were used to control the overall geometry of the constructed cross-sections.

VOL. 18, NO. 4, FEBRUARY 2023 ISSN 1819-6608
ARPN Journal of Engineering and Applied Sciences

www.arpnjournals.com

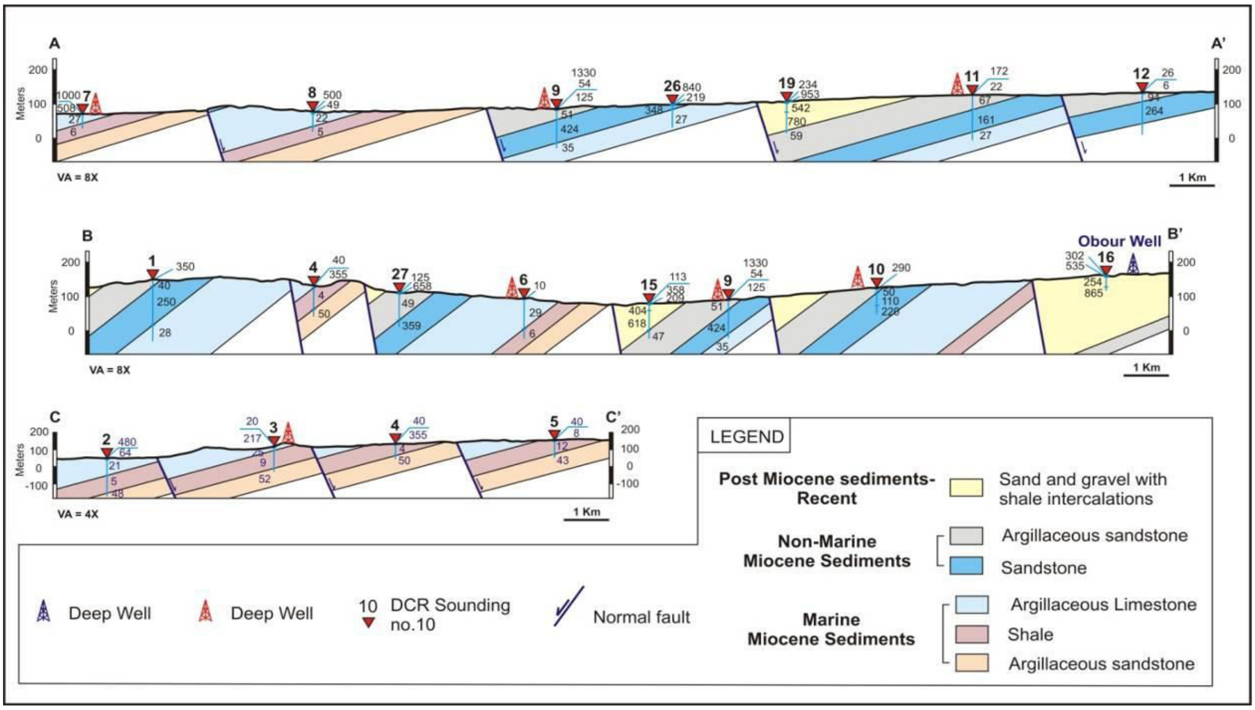

Figure-6. Stitched resistivity sections (A-A', B-B' and C-C') of the inverted DCR soundings (for location, c.f. Figure-1b) considering outcrop, structural and borehole data. Note, the trends of geoelectrical sections are represents in Figure-1b as white dashed lines.

Figure-6 shows a wide variation in geoelectrical layer resistivity values and thicknesses in both horizontal and vertical directions revealing lithological heterogeneities and/or various structural changes. With detailed surface structural mapping and borehole data, the constructed cross-sections can be considered informative for controlling subsurface geological and structural mapping. In this manner, all surface mapped faults (Figure-4) are projected on the constructed stitched resistivity sections (A-A', B-B', and C-C'). The near-surface layer (i.e., first geoelectrical layer) represents a wide range of resistivities (6-1330 ohm-m) corresponding to undifferentiated deposits constituting the desert varnish and loose sediments of clay, shale, sand, gravelly sand and gravel. Notably, the measured DCR soundings at the western and southwestern parts (e.g., DCR soundings No. 4, 7, 8) of the study site are characterized by medium (21-52 ohm-m) to low resistivity (< 10) values corresponding to marine Miocene sediments. It can be noticed that the marine Miocene sediments are mainly composed of three units: the shallowest unit shows medium resistivity values ranging from 21 to 35 ohm-m, which can be attributed to argillaceous limestone; the second geoelectrical unit represents low resistivity values (< 10) corresponding to marine shale layer; the third unit represents medium resistivity values (43-52 ohm-m), which corresponds to argillaceous sandstone.

At the southern and eastern parts of the study site, medium to high resistivity (40-424 ohm-m) layers can be noticed in several DCR soundings (e.g., DCR soundings No. 10, 11, 12) corresponding to non-marine Miocene sediments. The A-A' and B-B' geoelectrical cross-sections indicate that the non-marine sediments are composed mainly of two geoelectrical units: The first unit represents medium resistivity layer (40-94 ohm-m) which can be interpreted to argillaceous sandstone; The second unit represent high resistivity layer (> 110 ohm-m, soundings No. 10) attributing to sandstone. On the other hand, at the southeastern part (Obour well and DCR sounding No. 16), a high resistivity layer (> 100 ohm-m) can be recognized corresponding to post-Miocene to recent sediments with thickness of more than 150 m

Considering the available borehole and surface structural data, the A-A', B-B' and C-C' geoelectrical cross-sections (Figure-6) shows lateral heterogeneities between the different lithologic units of marine Miocene, Non-marine Miocene and Post-Miocene sediments. Such lateral heterogeneities are notably shown as variations of thicknesses and resistivities. Considering the outcrop and borehole data with aid of the interpreted DCR soundings, the abrupt changes in layers resistivity values can be related to normal faults that cut through the different lithologic units. Such faults have been plotted on the geoelectrical cross-sections considering the outcrop measurements of fault surfaces. The assembled faults show variation of throws along the geoelectrical cross-sections which vary relative to the nature of juxtaposition according to the interpreted DCR soundings. For example, the faults run through the marine-Miocene sediments show throw values that range from 100-130 m (e.g., geoelectrical cross-section C-C'). On the other hand, throws along fault planes show high values where marine-Miocene sediments are juxtaposed against non-marine or post-Miocene sediments (e.g., geoelectrical cross-sections

ARPN Journal of Engineering and Applied Sciences

A-A' and B-B'). The measured throws along the latter faults usually exceed 200 m and reach about 600 m.

Particularly, the extracted geological and structural data from field mapping and DCR interpretation were projected together on the constructed detailed geological map, Figure-7. The projection of geological and structural data was controlled by the deduced geometrical parameters of bedding planes and faults attitudes. Accordingly, the projected subsurface faults revealed new fault segments as well as merged segment extensions for surface mapped faults. A sum of fifteen mapped fault segments were plotted and analyzed where they belong to two main prominent sets which are NE-SW and NW-SE orientations (Figure-7).

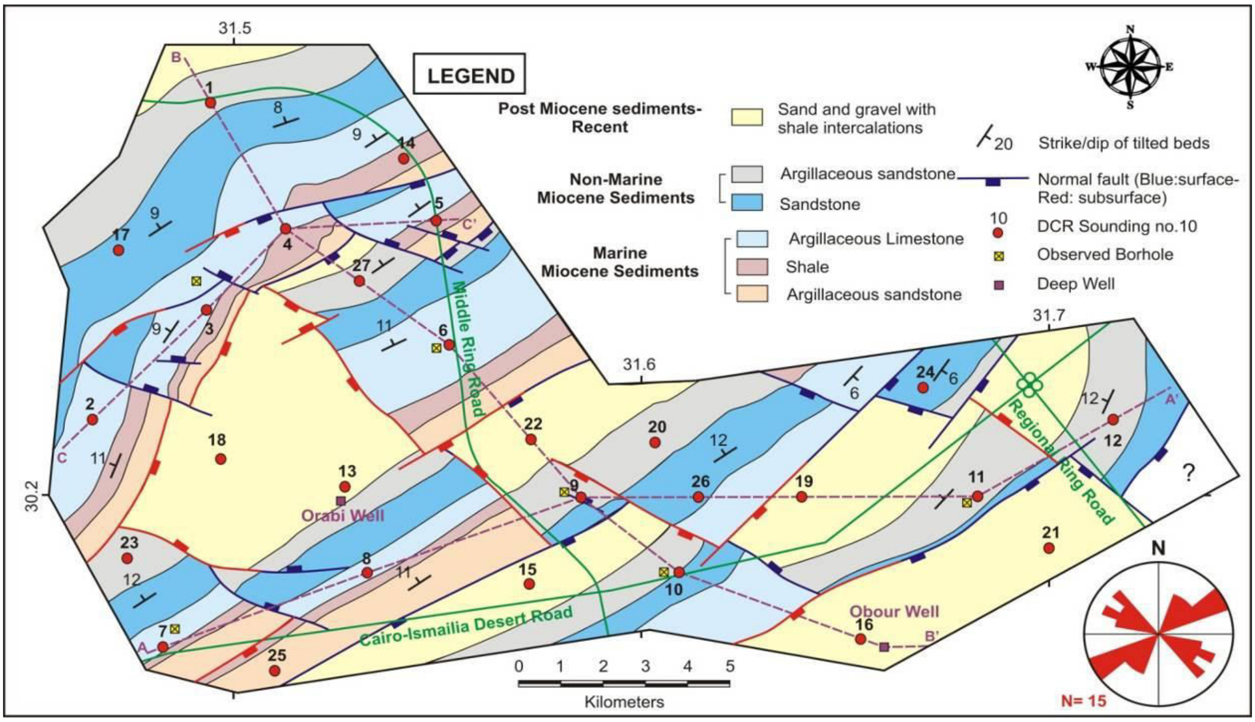

Figure-7. A high precision mapping for the study area. Lithologic layers of each rock unit is mapped separately, also, subsurface deduced faults are projected (red fault symbol) and their attitudes are represented by a rose diagram.

Regarding the constructed detailed geological mapping (Figure-7), the urban geological hazards can be assessed and/or managed. Obviously, the integration of surface geological and DCR data is essential to construct a robust and/or detailed geological map of the study site. Moreover, DCR method in the form of the DCR soundings has a pivotal role to acquire regional subsurface geological and structural information. However, more detailed structural imaging is required to refine the detailed urban geological mapping (Figure-7) including characterization procedures of the internal architecture of the deduced normal faults. (49), (14) indicated that the geophysical tomography complemented with 1D geophysical survey, outcrop and borehole data is an optimized and fast approach to refine urban geological mapping and fault zone characterization in desert lands. Accordingly, adding 2D information to traditional 1D resistivity survey and geological data can improve the knowledge of subsoil heterogeneities for preliminary engineering investigations amidst reclaiming desert-land. Consequently, electrical resistivity tomography (ERT) is recommended to refine the constructed urban geological mapping by imaging fault zones and delineating the near-surface faults geometry in the urban areas.

4.2 Implications: Preliminary Geohazards Recognition

Nowadays, urban geological mapping is considered as a specific stage which be critically considered, especially, when dealing with high deformed areas as in the present study. Regarding to the abovementioned surface and subsurface geological mapping, the study site is characterized by faults and shale layers presence. From an engineering point of view, undesirable of engineering problems may take place in dramatic ways related to such faults and shale layers (50), (51). From this perspective, fault rupture hazards are considered one of the main critical factors in planning that should be avoided through highly faulted zones. Additionally, fault rupture may tilt and/or damage buildings on or around the fault trace. Consequently, integration of outcrop and geophysical methods is necessary in order to delineate surface and near surface faults accurately. In this manner, the assembled data of the mapped faults have been gathered (Table-1) and used for calculating fault setbacks (Figure-8).

In the present study, the mapped faults have been merged and numbered (Figure-8a). In addition, fault setbacks have been calculated for both up thrown and downthrown sides (Table-1) around the mapped fault traces considering the geometric parameters of the fault traces using the following equations (52) (Figure-8b):

a) Downthrown Fault Block (Hanging Wall)

$$S = U\,(2D + F/\tan\Theta) \quad (1)$$

b) Upthrown Fault Block (Footwall)

$$S = U \times 2D, \quad (2)$$

where, S, U, D, F and Θ are the setback, criticality factor, fault displacement, maximum depth of sub-grade portion of the structure and fault dip, respectively.

The maximum fault throw values along each fault trace are herein used. Moreover, fault setbacks (S1, S2, S3) are calculated considering the criticality factors (U= 1, 2 and 3) and type of occupancy according to (53) (where, U=1 is used for storage and utility occupancy; U=2 is used for assembly, business and industrial occupancy; U=3 is used for educational and institutional occupancy). The provided results in Table-1 introduce a preliminary catalogue for planning engineers and decision makers in order to avoid future uncontrolled fault rupture hazards. Nevertheless, it is highly recommended that a seismic catalogue of earthquake events should be also considered in order to be aware of the active faults hazard at the area.

From geological point view, the Miocene shale layer intercalations are dominant in other new communities along CSD (e.g. Al Shorouk and Badr cities, for location, c.f. Figure-1a). From engineering point of view, such shale layer may cause geohazards (54) including expansion, collapse and low bearing capacity that may cause geotechnical and civil difficulties (e.g. water logging). Consequently, the mapping and geotechnical characterization of shale layers are highly required. In the study site, information coming from field observations (Figure-1c and Figure-3), surface geological mapping (Figure-4) and DCR sounding inversion results (Figure-6) depicted a clear picture of the shale layers distribution. Accordingly, the integration of surface and subsurface data allowed us to map the shale layers in high resolution image. For a particular first hand geohazard recognition, the physical shale layer property was carried out including free swelling (FS) test on ten collected samples. The laboratory results showed that the FS percent ranged from 180 % to 240 %. Accordingly, the shale layer has high sensitivity for swelling (Egyptian code 2001). Generally speaking, the swelling sensitivity refers to volume change probability for these fine soils in presence of water. Consequently, water logging can be expected as an environmental-engineering problem, which may cause collapsed/ cracked road pavements. It is worth mentioned that, the water logging problem and tilted buildings were observed in many new urban communities along CSD related to shale layers presence (55). Accordingly, the preliminary knowledge of geo-engineering hazards related to shale layer soil is represented on the first evaluation round of the urbanism expansion in desert lands. Regarding to preliminary geotechnical assessment, it is worth mentioning that the study site can be considered as highly risky especially with faults and shale layers dominance. Because the detailed geotechnical study is beyond the present paper scope, geo-engineering considerations for urban planning and development process should be taken into account that might need extra efforts.

VOL. 18, NO. 4, FEBRUARY 2023 ISSN 1819-6608
ARPN Journal of Engineering and Applied Sciences

www.arpnjournals.com

Table-1. Structural parameters and calculated setback values for both up thrown and downthrown sides of the mapped faults. Note, S1, S2 and S3 are the calculated setback values regading to the criticality factors (U= 1, 2 and 3), respectively, according to (53).

Fault Number	Strike	Length (Km)	Displace ment "D" (m)	Downthrown Side Setback (S)			Up thrown Side Setback (S)		
				S1 (m)	S2 (m)	S3 (m)	S1 (m)	S2 (m)	S3 (m)
1	71	6.7	90	185	370	555	180	360	540
2	54	4.6	95	195	390	585	190	380	570
3	32	4.5	565	1135	2270	3405	1130	2260	3390
4	26	3.2	580	1165	2330	3495	1160	2320	3480
5	64	2.8	570	1145	2290	3435	1140	2280	3420
6	62	1.5	70	145	290	435	140	280	420
7	52	0.7	300	605	1210	1815	600	1200	1800
8	273	0.8	20	45	90	135	40	80	120
9	288	2.0	30	65	130	195	60	120	180
10	292	3.7	110	225	450	675	220	440	660
11	299	1.7	400	805	1610	2415	800	1600	2400
12	293	1.5	50	105	210	315	100	200	300
13	291	3.3	50	105	210	315	100	200	300
14	90	5.7	120	245	490	735	240	480	720
15	293	3.2	180	365	730	1095	360	720	1080
16	57	2.8	35	75	150	225	70	140	210
17	320	4.0	420	845	1690	2535	840	1680	2520
18	58	5.3	610	1225	2450	3675	1220	2440	3660
19	315	3.5	310	625	1250	1875	620	1240	1860
20	297	0.9	40	85	170	255	80	160	240
21	299	4.5	110	225	450	675	220	440	660
22	61	9.4	560	1125	2250	3375	1120	2240	3360
23	294	2.6	250	505	1010	1515	500	1000	1500
24	45	7.5	290	585	1170	1755	580	1160	1740
25	300	2.6	180	365	730	1095	360	720	1080
26	74	1.9	120	245	490	735	240	480	720
27	37	3.3	170	345	690	1035	340	680	1020
28	308	2.6	130	265	530	795	260	520	780
29	61	10	240	485	970	1455	480	960	1440
30	310	2.5	150	305	610	915	300	600	900

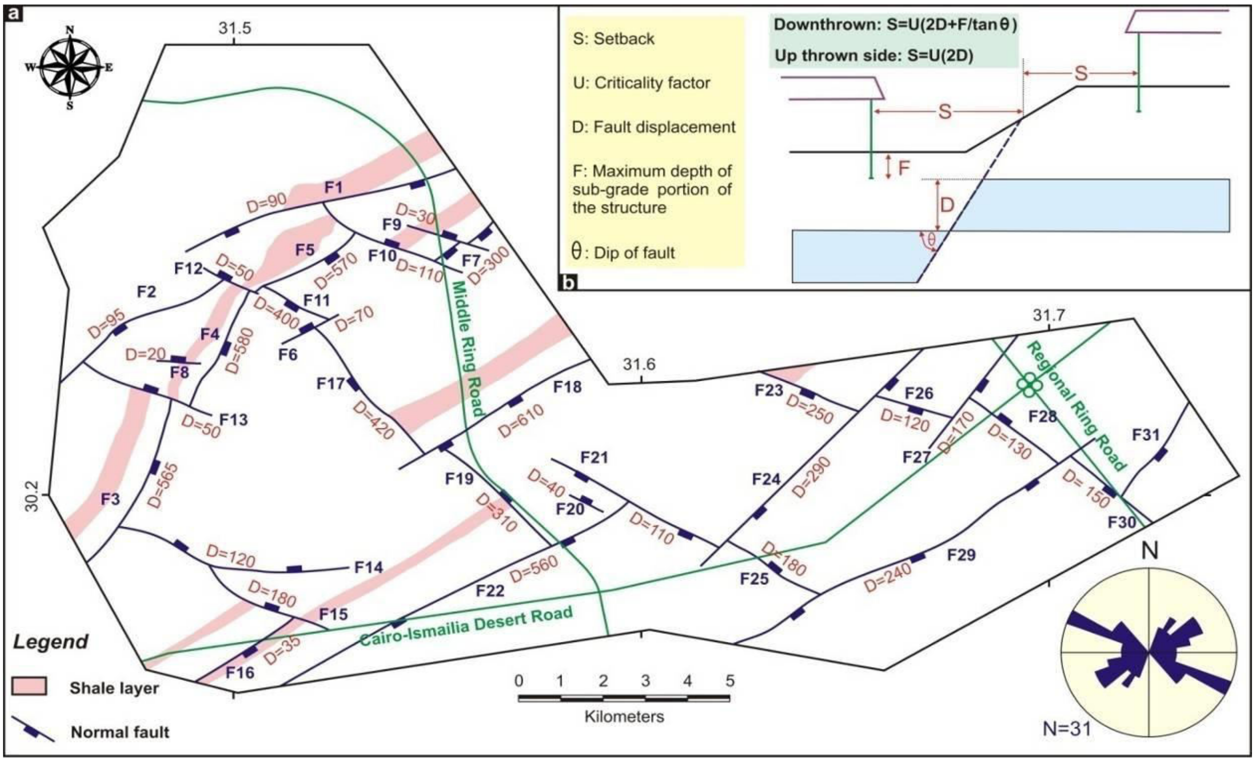

Figure-8. (a) A map shows the distribution of the shale layers (FS ranges from 180-240%) and all the deduced faults with a rose diagram representing their attitudes at the present study. (b) Setback variables for both the downthrown and up thrown sides of the fault plane (52), for calculated setback vlaues, c.f., Table-1.

5. CONCLUSIONS

Urban geology concerns the study of geologic environments and hazards for urban planning and development. With no detailed geological and structural data for sustainable urban planning, urban expansion and construction can impose additional geohazards related to problematic soils and near-surface structures. In the present exemplary study, an integrated approach was introduced of outcrop, DCR and borehole data for detailed mapping of surface as well as near-surface geology in a highly deformed area (i.e., New Obour City). The present study with an integrated approach for a detailed structural mapping is the first attempt in a new city, New Obour City, Egypt, and has been adopted to highlight the importance of outcrop as well as near-surface geological investigations when dealing with urban geological mapping.

Outcrop and structural measurements were extracted through the field-work, where they were used with satellite image data to prepare geological and structural maps. The inversion results of DCR soundings applying linear and non-linear inversion schemes were congruous with the borehole and surface structural data. Three problem-solving cross sections were prepared using a merge of outcrop, DCR and borehole data. The constructed geoelectrical cross-sections showed detailed subsurface layers distribution and complex structures by constraining DCR soundings inversion though a prior geological and structural geometric parameters to increase the reliability of the constructed models. It can be noticed that DCR soundings inversion with geological and structural constrains reduces the commonly known DCR sounding limitations. Moreover, the near-surface shale layers which are commonly represented at the northern and western parts of the study site constituting, in turn, instant engineering concern (IEC). As a result, the DCR sounding saves time and it is inexpensive method and easy to carry out in comparison with the conventional drilling for new urbanism and new cities planning in desert lands.

From an engineering point view, primary geotechnical risks were assessed by carrying out the FS test on shale soil samples and calculating the fault setbacks of the deduced faults. The results of shale swelling potentiality indicated that engineering construction precautions have to be considered to avoid the environmental and geo-engineering problems related to water logging and increasing salinity within the near-surface soil. Fault setbacks were calculated for both hanging walls and footwalls of the mapped faults considering the maximum throw along each fault and the measured dip angles of fault planes. Obviously, three values of criticality factor were used according to the nature of the building type. Regarding the above mentioning conclusions, the suggested approach can provide a preliminary geotechnical scheme for engineers and decision makers prior to planning. However, further geotechnical parameters of problematic lithologic layers (e.g. shale) are obligatory outputs which enhance the urban mapping and hence, offer additional precision for sustainable planning. Regarding the present work results, we came to the following conclusions:

- Incorporation of outcrop, multi-scale geophysical methods and borehole data are necessary for high reliability urban geological mapping.
- While surface geological mapping is essential for a first hand geohazard assessment, information extracted from DCR inversion results allows portraying the main near-surface geology in low cost strategy.
- The DCR soundings show a great importance for large scale geological surveys, which are mandatory for detailed near-surface structural and lithologic mapping.
- Structural complexity and seismicity should be considered in urban geological mapping. Consequently, calculation of fault setbacks are highly recommended as a mandatory step for urban planning to avoid future complicated geohazards as fault reactivation.

ACKNOWLEDGEMENTS

Special thanks go to A.T. Basokur and I. Akca (Ankara Uni. Turkey) for great support and assistance with inversion software during preparing this paper. The authors would also like to express appreciation to Structural Geophysics Group (SGG) members, Zagazig University, Egypt, for great support, valuable discussions and assistance with data collection during this work.

REFERENCES

Elsawy MBD, Lakhouit A. 2020. A review on the impact of salinity on foundation soil of coastal infrastructures and its implications to north of Red Sea coastal constructions. Arabian Journal of Geosciences, 13, 555. https://doi.org/10.1007/s12517-020-05601-6

United Nations. 2019. The Sustainable Development Goals Report, p 61. https://doi.org/10.18356/55eb9109-en

El May M., Dlala M., Chenini I. 2010. Urban geological mapping: Geotechnical data analysis for rational development planning, Engineering Geology, 116, 129-138 https://doi.org/10.1016/j.enggeo.2010.08.002.

Marker BR, Pereira JJ, de Mulder EEJ. 2003. Integrating Geological Information into Urban Planning and Management: Approaches for the 21st Century. Earth Science in the City: A Reader, p 379. https://doi.org/10.1029/SP056p0379

Cappadonia C., Di Maggio C., Agate M., Agnesi V. 2020 Geomorphology of the urban area of Palermo (Italy). Journal of Maps, 16(2): 274-284. https://doi.org/10.1080/17445647.2020.1739154

Poyiadji E., Kontogianni V., Nikolaou N. 2017. Integration of geohazards in urban planning and management. Advanced Engineering Forum, ISSN: 2234-991X 21:557-563. https://doi.org/10.4028/www.scientific.net/AEF.21.557

Henaish A., Attwa M. 2018. Internal structural architecture of a soft-linkage transfer zone using outcrop and DC resistivity data: Implications for preliminary engineering assessment. Engineering Geology, 244: 1-13. https://doi.org/10.1016/j.enggeo.2018.07.018

Sakran S.M., Nabih M., Henaish A., Ziko A. O. 2016. Fracture reopening by micro-earthquakes, a mechanism for oil seepage in mildly active rifts: a Case study from Gemsa oil field, the southern Gulf of Suez rift, Egypt. Arabian Journal of Geosciences. 9(5): 1-17.

Khalifa A., Bashir B., Çakir Z., Kaya Ş., Alsalman A., Henaish A. 2021. Paradigm of Geological Mapping of the Adıyaman Fault Zone of Eastern Turkey Using Landsat 8 Remotely Sensed Data Coupled with PCA, ICA, and MNFA Techniques. ISPRS International Journal of Geo-Information, 10(6): 368. https://doi.org/10.3390/ijgi10060368

Lyu H-M, Shen JS, Arulrajah A. 2018. Assessment of Geohazards and Preventative Countermeasures Using AHP Incorporated with GIS in Lanzhou, China. Sustainability. 10(2): 304. https://doi.org/10.3390/su10020304

Wang H., Li C. 2021. Analysis of scale effect and change characteristics of ecological landscape pattern in urban waters. Arabian Journal of Geosciences, 14, 569. https://doi.org/10.1007/s12517-021-06831-y

Alkaradaghi K., Ali SS, Al-Ansari N., Laue J., Chabuk A. 2019. Landfill site selection Using MCDM methods and GIS in the Sulaimaniyah Governorate, Iraq. Sustainability, 11(17): 4530. https://doi.org/10.3390/su11174530

El-Saadawy O., Gaber A., Othman A., Abotalib AZ, El Bastawesy M., Attwa M. 2020. Modeling flash floods and induced recharge into alluvial aquifers using multi-temporal remote sensing and electrical resistivity imaging. Sustainability. 12(23): 10204. https://doi.org/10.3390/su122310204

Attwa M., Henaish A., Zamzam S. 2020. Hydrogeologic characterization of a fault-related dome Using outcrop, borehole and electrical resistivity data. Natural Resources Research, 29(2): 1143-1161. https://doi.org/10.1007/s11053-019-09504-6

Akca I., Gölebatmaz SM. 2021. Three-dimensional inversion of DCR data incorporating structural similarity constraint. Journalof Applied Geophysics, 184, 104237. https://doi.org/10.1016/j.jappgeo.2020.104237

Fatma K., Yacine D., Haydar B., *et al*. 2020. Use of electrical resistivity tomography (ERT) and electromagnetic induction (EMI) methods to Characterize Karst Hazards in north-eastern of Algeria. Arabian Journal of Geosciences, 13, 1204. https://doi.org/10.1007/s12517-020-06206-9.

Perrone A., Lapenna V., Piscitelli S. 2014. Electrical resistivity tomography technique for landslide investigation: A review. Earth-Science Reviews, 135, 65-82. https://doi.org/10.1016/j.earscirev.2014.04.002.

Lawal A., Tijani MN, D'Alessio M. 2020. Geoelectrical characterisation of aquifers in Bauchi-Alkaleri-Kirfi geological transition zones, Northeast Nigeria. Environmental Earth Sciences, 79, 224. https://doi.org/10.1007/s12665-020-08978-5

Niculescu BM, Andrei G. 2021. Application of electrical resistivity tomography for imaging seawater intrusion in a coastal aquifer. Acta Geophysica, 69, 613-630. https://doi.org/10.1007/s11600-020-00529-7

El Bastawesy M., Gebremichael E., Sultan M., Attwa M., Sahour H. 2020. Tracing Holocene channels and landforms of the Nile Delta through integration of early elevation, geophysical, and sediment core data. The Holocene, 30(8): 1129-1141. doi:10.1177/0959683620913928

Zhao Y., Yu Y., Yang H., *et al*. 2021. Vertical electric soundings characteristics of paleochannel in the Yuyao River Valley, Eastern China. Bulletin of Engineering Geology and the Environment, 80, 1047-1061. https://doi.org/10.1007/s10064-020-01951-3

Attwa M., Henaish A. 2018. Regional structural mapping using a combined geological and geophysical approach - A preliminary study at Cairo-Suez district, Egypt. Journal of African Earth Sciences, 144, 104-121. https://doi.org/10.1016/j.jafrearsci.2018.04.010

Hagag W. 2016. Structural evolution and Cenozoic tectonostratigraphy of the Cairo-Suez district, north Eastern Desert of Egypt: Field-structural data from Gebel Qattamiya-Gebel Um Reheiat area. Journal of African Earth Sciences. 118, 174-191.

Henaish A. 2018a. Soft-linkage transfer zones: Insights from the Northern Eastern Desert, Egypt. Marine and Petroleum Geology, 95, 265-275. https://doi.org/10.1016/j.marpetgeo.2018.05.005

Henaish A. (2018b). Fault-related domes: Insights from sedimentary outcrops at the northern tip of the Gulf of Suez rift, Egypt. Marine and Petroleum Geology, 91, 202-210. https://doi.org/10.1016/j.marpetgeo.2018.01.009

Kharbish S., Henaish A. and Zamzam S. Geodiversity and geotourism in Greater Cairo area, Egypt: implications for geoheritage revival and sustainable development. Arabian Journal of Geosciences, 13, 451. https://doi.org/10.1007/s12517-020-05457-w

Meshref WM. 1990. Tectonic framework of Egypt. In: Said R, ed. The geology of Egypt. Balkema, Rotterdam, Netherlands, 133-155.

Guiraud R., Bosworth W. 1997. Senonian basin inversion and rejuvenation of rifting in Africa and Arabia: synthesis and implications to plate-scale tectonics. Tectonophysics. 282, 39-82.

Guiraud R., Bosworth W. 1999. Phanerozoic geodynamic evolution of northeastern Africa and the northwestern Arabian platform. Tectonophysics. 315, 73-108.

Moustafa AR, Abd-Allah MA. 1992. Transfer zones with en echelon faulting at the northern end of the Suez rift. Tectonics. 11, 499-509.

Moustafa AR, El Badrawy R., Gibali H. 1998. Pervasive E-ENE oriented faults in northern Egypt and their effect on the development and inversion of prolific sedimentary basins. In: 14th E.G.P.C. Petrol. Conf. Cairo. 1, 51-67.

Moustafa AR. 2002. Controls on the geometry of transfer zones in the Suez rift and northwest Red Sea: Implications for the structural geometry of rift systems. AAPG Bulletin. 86, 979-1002.

Henaish A., Kharbish S. 2020. Linkage style of rift-associated fault arrays: insights from central Cairo-Suez district, Egypt. Carpathian Journal of Earth and Environmental Sciences, February 2020, 15(1): 189-196.

Abou Elenean KM, Mohamed AME, Hussein HM. 2010. Source parameters and ground motion of the Suez-Cairo shear zone earthquakes, Eastern Desert, Egypt. Natural Hazards. 52, 431-451.

Issawi B., Sallam ES, Salem M. 2018. Tectonostratigraphic and sedimentary evolution of the Ubur-Orabi sub-basin, southeast Nile Delta, Egypt. Carbonates and Evaporites, 33, 663-681. https://doi.org/10.1007/s13146-017-0392-z

Shukri NM, Akmal MG. 1953. The geology of Gebel El Nasuri and Gebel El-Anqabiya district. Bulletin de la Société de géographie d'Egypte. 26, 243-276.

Moustafa AR, Yehia MA, Abdel Tawab S. 1985. Structural setting of the area east of Cairo, Maadi, and Helwan. Middle East Research Center, Ain Shams University, Earth Science Series. 5, 40-64.

Moustafa AR, Abd-Allah MA. 1991. Structural setting of the central part of the Cairo-Suez District. Middle East Research Center, Ain Shams University, Earth Science Series. 5, 133-145.

Gouasmia, M., Khorchani, H., Mhamdi A., *et al*. 2018. Hydrogeological characterization of a carbonate

ARPN Journal of Engineering and Applied Sciences

aquifer using geophysical and geochemical approach: case of the Krachoua Formation in Tataouine area, Southern Tunisia. Arabian Journal of Geosciences, 11, 786. https://doi.org/10.1007/s12517-018-4150-x

Attwa M., El Bastawesy M., Ragab D., Othman A., Assaggaf HM, Abotalib AZ. 2021a. Toward an integrated and sustainable water resources management in structurally-controlled watersheds in desert environments using geophysical and remote sensing methods. Sustainability, 13(7): 4004. https://doi.org/10.3390/su13074004.

Yilmaz S. 2011. A case study of the application of electrical resistivity imaging for investigation of a landslide along highway. International Journal of Physical Sciences, 6(24): 5843-5849. DOI: 10.5897/IJPS11.564

El Bastawesy M., Attwa M., Abdel Hafeez TH, Gad A. 2019. Flash floods and groundwater evaluation for the non-gauged dryland catchment using remote sensing, GIS and DC resistivity data: A case study from the Eastern Desert of Egypt. Journal of African Earth Sciences, 152, 245-255. DOI 10.1016/j.jafrearsci.2019.02.004

Ebong ED, Abong, AA, Ulem EB *et al*. 2021. Geoelectrical resistivity and geological characterization of hydrostructures for groundwater resource appraisal in the Obudu Plateau, southeastern Nigeria. Natural Resources Research, 30, 2103-2117. https://doi.org/10.1007/s11053-021-09818-4

Basokur AT. 1999. Automated 1D interpretation of resistivity soundings by simultaneous use of the direct and iterative methods. Geophysical Prospecting. 47, 149-177.

Basokur AT, Akça I, Siyam NWA. 2007. Hybrid genetic algorithms in view of the evolution theories with application for the electrical sounding method. Geophysical Prospecting. 55, 393-406.

Akça I., Basokur AT. 2010. Extraction of structure-based geoelectric models by hybrid genetic algorithms. Geophysics. 75, 15-22.

Attwa M., El Mahmoudi A., Elshennawey A.., *et al*. 2021b. Soil Characterization Using Joint Interpretation of Remote Sensing, Resistivity and Induced Polarization Data along the Coast of the Nile Delta. Natural Resourources Research, 30, 3407-3428. https://doi.org/10.1007/s11053-021-09883-9

Goldberg DE. 1989. Genetic Algorithms in Search, Optimization and Machine Learning. Addison-Wesley, Boston, Mass.

Gaba`s A., Macau A., Benjumea B., Bellmunt F., Figueras S., Vila M. 2014. Combination of Geophysical Methods to Support Urban Geological Mapping. Surveys in Geophysics, 35, 983-1002. DOI 10.1007/s10712-013-9248-9

Attwa M., El-Shinawi A. 2017. An integrative approach for preliminary environmental engineering investigations amidst reclaiming desert-land: a case study at East Nile Delta, Egypt. Environmental Earth Sciences. 76(8): 304.

Sun L, Liu Q., Grasselli G., Tang X. 2020. Simulation of thermal cracking in anisotropic shale formations using the combined finite-discrete element method. Computers and Geotechnics. 117, 103237.

Batatian D. 2002. Minimum Standards for Surface Fault Rupture Hazard Studies. Salt Lake County Geologic Hazards Ordinance, Appendix A. p. 11.

International Code Council. 2000. International building code. International Code Council. p. 297.

Saad A. 2013. Geological, Soil and Rock Mass Evaluation for Risk Assessment of Badr City, Egypt. Middle East Journal of Applied Sciences. 3(4): 265-276.

Massoud M, M. Khalil MM, Tokunaga T, Santos FAM. 2015. Preliminary hydrogeophysical investigation at the 10th of Ramadan City, Egypt, by 1D and 2D inversion of VES data. Near Surface Geophysics, 14(3): 287-297. https://doi.org/10.3997/1873-0604.2016005